A&A 475, 991–1002 (2007)
DOI: 10.1051/0004-6361:20078267

Astronomy & Astrophysics

A search for solar-like oscillations in K giants in the globular cluster M 4⋆

S. Frandsen[1], H. Bruntt[1,2], F. Grundahl[1,3], G. Kopacki[4], H. Kjeldsen[1,3], T. Arentoft[1,3], D. Stello[2], T. R. Bedding[2], A. P. Jacob[2], R. L. Gilliland[5], P. D. Edmonds[6], E. Michel[7], and J. Matthiesen[1]

[1] Department of Physics and Astronomy, University of Aarhus, Ny Munkegade, Bygn. 520, 8000 Aarhus, Denmark
e-mail: srf@phys.au.dk
[2] School of Physics A28, University of Sydney, 2006 NSW, Australia
[3] Danish AsteroSeismology Center (DASC), University of Aarhus, 8000 Aarhus, Denmark
[4] Institute of Astronomy, University of Wrocław, Poland
[5] Space Telescope Science Institute, Baltimore, USA
[6] Center for Astrophysics, Cambridge, MA, USA
[7] Observatoire de Paris, Meudon, France

Received 13 July 2007 / Accepted 10 August 2007

ABSTRACT

Context. To expand the range in the colour–magnitude diagram where asteroseismology can be applied, we organized a photometry campaign to find evidence for solar-like oscillations in giant stars in the globular cluster M 4.
Aims. The aim was to detect the comb-like p-mode structure characteristic for solar-like oscillations in the amplitude spectra. The 24 main target stars are in the region of the bump stars and have luminosities in the range 50−140 $L_{\odot}$.
Methods. We collected 6160 CCD frames and light curves for about 14 000 stars were extracted. The frames consist of exposures in the Johnson B, V and R bands and were obtained at three different telescopes. Three different software packages were applied to obtain the lowest possible photometric noise level. The resulting light curves have been analysed for signatures of oscillations using a variety of methods.
Results. We obtain high quality light curves for the K giants, but no clear oscillation signal is detected. This is a surprise as the noise levels achieved in the amplitude spectra should permit oscillations to be seen at the levels predicted by extrapolating from stars at lower luminosities. In particular, when we search for the signature of oscillations in a large number of stars we might expect to see common features in the power spectra, but even here we fall short of having clear evidence of oscillations.
Conclusions. High precision differential photometry is possible even in very crowded regions like the core of M 4. Solar-like oscillations are probably present in K giants, but the amplitudes are lower than classical scaling laws predict. The reasons may be that the lifetime of the modes are short or the driving mechanism is relatively inefficient in giant stars.

Key words. stars: oscillations – stars: activity – techniques: photometric – methods: observational – stars: evolution

1. Introduction

Asteroseismology has made great progress in recent years due to improved observational techniques. Extremely stable spectrographs have been designed to detect exo-planets through Doppler shifts. These instruments have allowed the unambiguous detection of p-modes in about a dozen solar-type stars (for a review see Bedding & Kjeldsen 2007). Although most results have been obtained for main-sequence and subgiant stars, some giant stars have also been shown to oscillate: ξ Hya (G7III; Frandsen et al. 2002), ϵ Oph (G9.5III; De Ridder et al. 2006a; Barban et al. 2007), and η Ser (K0III; Barban et al. 2004). Unambiguous detection of p-modes has so far been restricted to field stars in our immediate neighbourhood.

Döllinger et al. (2005) found that field stars show radial velocity and photometric variability, which seems to increase with increasing luminosity. This could either be due to a combination of activity and granulation, or to pulsations, either self-excited (Mira-like) or driven by convective motions (solar-like). Similar evidence for increased variability has been found for stars in the globular cluster 47 Tucanae (Edmonds & Gilliland 1996).

Stellar clusters present a highly interesting prospect, due to the large number of stars collected in a limited field of view and additional constraints from cluster properties, such as relative age, metallicity, and evolutionary stage. Gilliland et al. (1993) were the first to make a search for solar-like oscillations in the main sequence F-type stars in the open cluster M 67. However, based on their multi-site campaign using 4-m class telescopes they made no clear detection. Recently, another campaign was carried out on the same cluster (Stello et al. 2006b, 2007), this time concentrating on stars on the lower part of the giant branch, where larger oscillation amplitudes are expected.

Knowing that p-modes are excited in giant stars, we decided to study K giants in the globular cluster M 4. The two main reasons are that M4 has a rich population of K giants (see Fig. 2) and the amplitudes are expected to be substantially higher than for subgiants. If we could measure the gross properties of the oscillations, such as amplitudes and the large splitting characteristic for solar-like oscillations, we could potentially study an ensemble of giant stars in different evolutionary stages.

⋆ Based on observations with the Danish 1.54 m on La Silla at the European Southern Observatory in Chile, the 1.5 m at Cerro Tololo Inter-American Observatory in Chile, and the SSO 40″ at Siding Spring Observatory in Australia.

Table 1. Observing log for the M 4 campaign in 2001.

	Number of images			Date of observation	
Observatory	*B*	*V*	*R*	Start	End
SSO	0	548	735	May 1	June 10
CTIO	143	274	446	June 1	June 6
La Silla	847	1358	1809	April 13	June 30

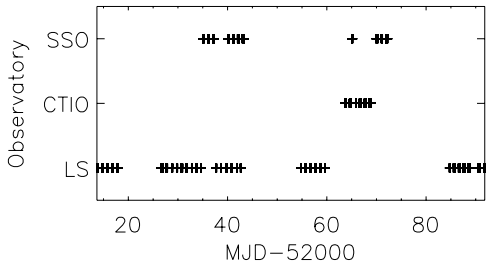

Fig. 1. Distribution of nights for the three observing sites. The time baseline is 78 days.

According to the empirical calibration by Kjeldsen & Bedding (1995), oscillation amplitudes scale as $L/(M\,T_{\rm eff}^2)$. For the K giants in M 4, taking the solar amplitude as 4.7 ppm (parts per million), we expect amplitudes in the range 400−1000 ppm. The noise level we expected to reach in the amplitude spectra for the bright giant stars was ≃25 ppm at high frequencies. This would allow us to detect any excess power, and possibly the comb-like structure of the *p*-modes, in the amplitude spectra for the brightest and least crowded targets. However, the mode frequencies decrease with luminosity and approach a range where noise caused by extinction and transparency changes is difficult to eliminate in ground-based data.

2. The observations

CCD frames were obtained with the Danish 1.54 m telescope at La Silla, the 1.5 m telescope at Cerro Tololo Inter-American Observatory (CTIO), both in Chile, and the 1 m telescope at the Siding Spring Observatory (SSO) in Australia. The observations took place over a period of almost three months, in order to get the necessary frequency resolution. We started at La Silla on April 13, 2001 and got the last data on June 27, 2001. We obtained useful data on 48 nights out of an allocation of 63 nights. Some nights had overlap between Australia and Chile, which we used to check the consistency of the photometric results. Table 1 gives a list of the collected dataset. In total we have 6160 CCD frames of M 4 (4014 from La Silla, 863 from CTIO, and 1283 from SSO). The time distribution is represented in Fig. 1, which includes 31 nights from La Silla, 6 nights from CTIO, and 11 nights from SSO.

To help identify the modes, we observed in three filters: *B*, *V* and *R*. Amplitude ratios between different colours can indicate which types of modes are present. To enhance the signal-to-noise ratio, the data can still be combined using an approximate scaling (Eq. (8)), since phase differences of *p*-modes between filters are small. About equal time was allocated to the three filters, giving more frames in *R* due to the shorter exposure times.

The exposure times were adjusted to give the best results for stars in the range $12.5 < V < 13.5$, which is the area of the RGB bump in M 4, as seen in Fig. 2. This meant typical exposure times at La Silla and CTIO of less than one minute in *V* and *R* and a few minutes in *B*, depending on seeing conditions. Exposure times at SSO were 2−4 min in *V* and 1−2 min in *R*. On average, this led to a mean duty cycle around 50%, since the readout time was 1−2 min.

3. CCD photometry techniques

The images were first calibrated by performing traditional bias subtraction and flat-fielding. In order to avoid nightly offsets, calibration frames were constructed for periods of several days, typically a week, and the same calibration frames were used for all images in that period. This point is quite important since the timescale of variability for the giant targets is in the range 9−31 h (see Sect. 5.1).

CCD non-linearity was considered, and in the case of the La Silla data it was corrected using the technique described by Stello et al. (2006b). The other cameras did not provide the same option for a correction and were assumed to be linear. We have not seen any evidence for non-linearity and, since we were able to find comparison stars with similar magnitudes in all cases, the influence of non-linearity should be negligible.

In Fig. 3 we present the calibrated CCD image that has been used as the reference image for the La Silla observations of M 4. The 24 K giant stars we selected for a detailed analysis are marked by boxes.

In order to achieve the highest possible photometric precision, we decided to use three different reduction programs, all of which have been successful in the past in producing high quality results: ISIS, DAOPHOT and MOMF. In the most crowded areas we expected ISIS (Alard & Lupton 1998; Alard 2000) to give the best results. In the less crowded areas we expected that DAOPHOT (Stetson 1987) would do best. Finally, we know that MOMF (Kjeldsen & Frandsen 1992) performs very well in fields with only mild crowding. All frames were reduced with ISIS and DAOPHOT and a subset of the *V* frames from La Silla were reduced with MOMF. Each of the three methods will be described in Sects. 3.1−3.3 and we compare the results in Sect. 3.4.

3.1. The image subtraction method (ISIS)

The main advantage of the difference-image technique is the ability to extract high precision photometry in the crowded regions near the core of M 4. In addition, any variations in airmass and transparency are removed to first order as a part of the image subtraction.

The image subtraction method ISIS (Alard & Lupton 1998; Alard 2000) was used by two members of the team independently (ISIS1 and ISIS2). For each filter and each observing site we selected the images with the best seeing to make the reference images. While ISIS2 only used a single reference image for each site and filter, ISIS1 used subsets of data from about one week.

For each observed image, we computed a kernel which describes the variations of the PSF across the image relative to the reference image. We then convolved the reference image with the kernel and subtracted this from the observed image. The resulting difference image will contain the signal that is intrinsically different from the reference image, e.g., cosmic ray hits, hot pixels, and variable stars.

In the first approach (ISIS1) only La Silla and CTIO data were included (Bruntt 2003). They were divided into five subsets and reduced separately. The reason for this was large differences in the positional angle of the CCD camera between different periods. We had problems using the photometry package that is part of ISIS. Instead, we modified the aperture photometry routine in DAOPHOT in order to be able to run it on the subtracted images, in particular allowing negative flux values. The necessary

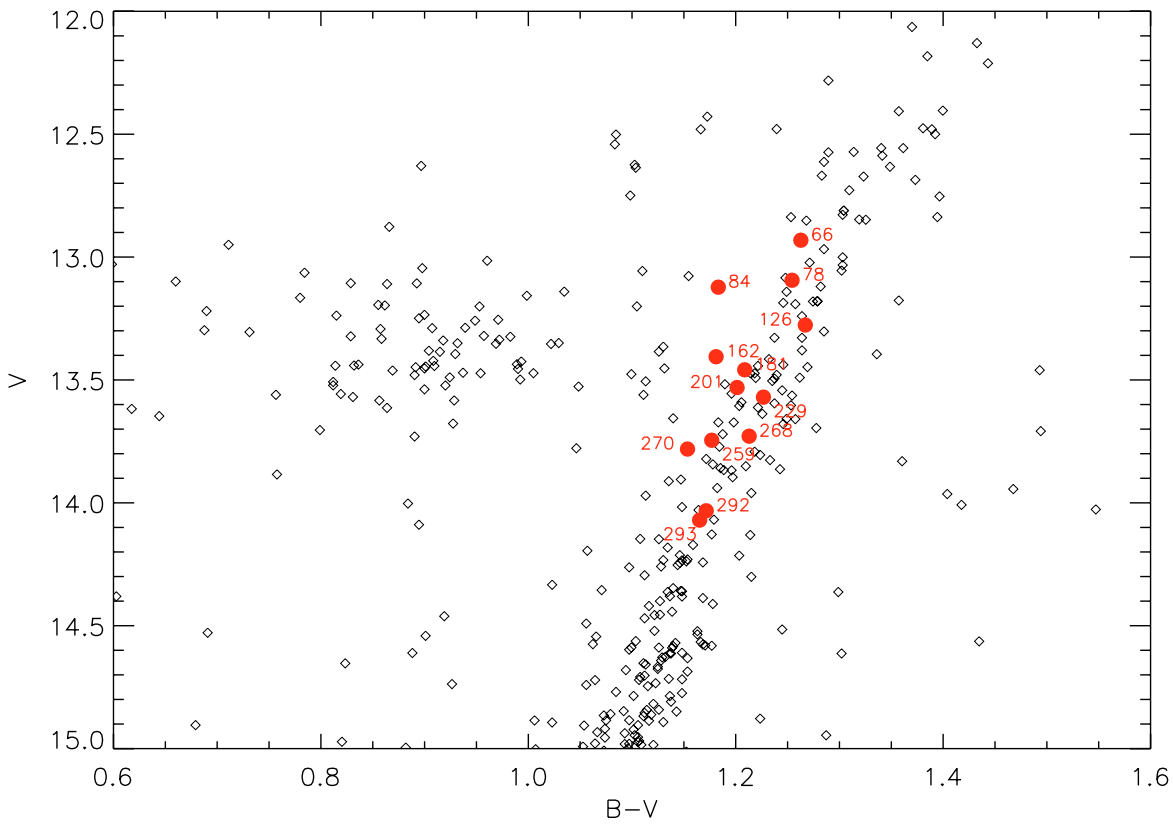

Fig. 2. The colour–magnitude diagram for M 4, showing the bump stars and part of the horizontal branch. The colours and magnitudes have been calibrated using the database provided by Stetson (2007). To show the range covered, some of the stars selected for a detailed analysis are indicated and labeled with the ID – see Table 2.

modifications were described in detail by Bruntt et al. (2003). ISIS needs a reference flux for each star, since only the change in the flux is calculated. This was taken from the DAOPHOT reduction of the reference images.

In the second reduction approach (ISIS2), we constructed only one reference frame for each observing site and passband. The original ISIS software does not work correctly with frames that are significantly rotated with respect to the reference frame. The problem resides in the interpolation process and we used our own application, which performs this task correctly even for large rotation angles but requires much more computation time. For all stars detected in the reference frames (for all three observing sites), we derived differential fluxes from our CCD frames following standard procedures of ISIS reductions (for details see Kopacki 2000). We performed both the PSF fitting and aperture photometry on the difference frames. To transform differential fluxes into magnitudes we used total fluxes measured in the reference frames using aperture photometry tasks NEDA+DAOGROW under DAOPHOT. Finally, all the data were merged into a uniform magnitude system by applying magnitude offsets determined from a carefully chosen set of bright unsaturated stars common to all three observing fields. In this way, the CTIO and SSO data were transformed into the magnitude scale of the La Silla data.

3.2. DAOPHOT/ALLSTAR/ALLFRAME reduction

For this reduction we used the suite of photometry programs developed by Stetson (1987, 1990, 1994): DAOPHOT, ALLSTAR and ALLFRAME. The general use of these is well described in manuals and the literature. For our applications we adopted a slightly modified procedure, as follows. Firstly, a few of the deepest and best-seeing frames were used to produce a master list of stars, which was obtained by several iterations through DAOPHOT, ALLSTAR and ALLFRAME. Next, all frames were run through DAOPHOT/ALLSTAR once. With the preliminary photometry in hand, positional transformations between each frame and our reference frame were derived using DAOMATCH and DAOMASTER (kindly provided by P. Stetson).

From the frames used to derive the master star list, we created two lists of stars for generating the PSF for the individual images. The first list contained ~10 stars that were well isolated and these were used to generate the first version of the PSF for each frame. Next the second list, containing ~200 stars covering the observed field, was used to generate the final PSF. We used this PSF when running ALLFRAME on all the images to produce the final photometry. We cross-identified all stars in the photometry files and selected the brightest 7000 for further analysis.

3.3. MOMF reduction

As an independent test we used the MOMF package (Kjeldsen & Frandsen 1992) on the La Silla images to derive time series in the V band. The reduction had to be done in a slightly different way than normal because the La Silla images were slightly rotated relative to each other. MOMF can only handle shifts and so introduced an additional coordinate transformation, changing the (x, y) coordinates for each image before doing photometry. For stars outside the very crowded regions, results were comparable to the other techniques. We conclude that we reach similar results for non-crowded regions by all of the techniques.

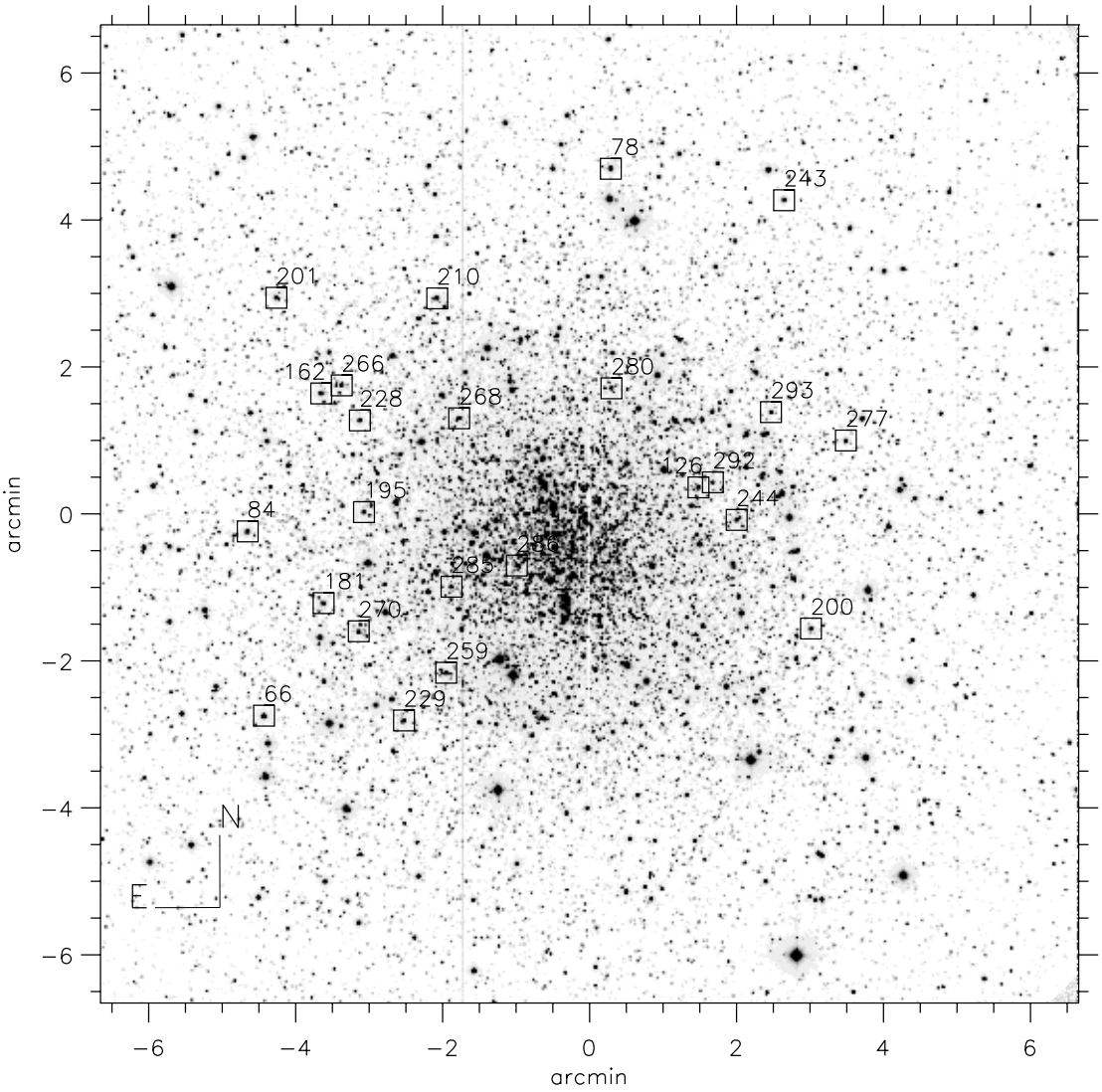

Fig. 3. The field of M 4 observed with the Danish 1.54 m telescope at La Silla. The 24 K giants we analysed in detail are marked by squares. The center of the field is at $\alpha_{2000} = 16^{\rm h}23^{\rm m}33\overset{\rm s}{.}7$, $\delta_{2000} = -26°31'05\overset{''}{.}7$.

3.4. Comparison of the photometry

Our database contains photometry from the three different reduction methods and comprises light curves of 13 611 stars with up to 6160 data points. We also store information about each frame such as seeing, airmass, background level, the mid-time of each observation (Julian date), and position on the reference frame of each star. The data can be accessed at the web page `http://astro.phys.au.dk/~srf/M4/`.

The rms scatter in the light curves is plotted versus magnitude for relatively good and bad nights in Figs. 4 and 5, respectively. These results are based on the ISIS1 photometry in the V-band. For the bad night, the noise is considerably larger than the good night for all stars. The higher noise is due to high sky background as a result of the close proximity of the Moon to M 4. The lower envelope of stars for the good night is close to the expected precision based on the flux level (indicated by the solid line). We find a number of stars with rms scatter as low as 1.5 mmag. For the K giants the level is typically about 2 mmag per data point. The *bump* stars are found around $V = 13.5$, where we obtain the lowest noise levels.

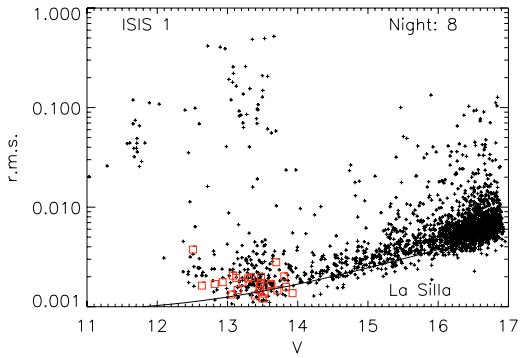

Fig. 4. The rms scatter around the mean for a good night with the Danish 1.54 m telescope, for the ISIS1 reduction. The red open squares give the noise level for the final time series for the selected K giants in which we have looked for solar-like oscillations. The line indicates the noise expected from scintillation and photon statistics. The stars with high scatter near $V = 13.3 \pm 0.3$ are RR Lyrae stars. Saturation sets in at $V \sim 12.5$.

As shown in Fig. 5, some nights do not give good results, with noise levels considerably higher than the majority of the data. Naturally, the noise per data point depends on the level of exposure per frame. This will vary as we had to adjust the

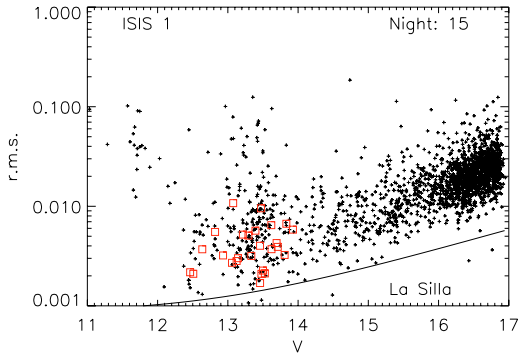

Fig. 5. Same as Fig. 4, but for a bad night that was characterized by very a large sky background due to moon light.

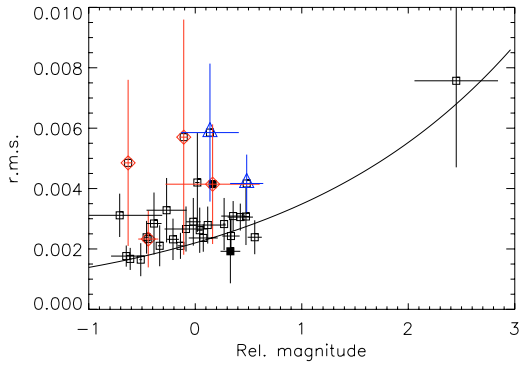

Fig. 6. The mean rms scatter per data point per night, plotted against the nightly mean flux level in the exposures represented by a corresponding magnitude difference between each night and a reference night. The filled symbols indicate two nights with very few observations. The overplotted diamonds indicate nights with a high sky level and the triangles show nights with very good seeing. The rms uncertainty is marked for each point.

exposure time to avoid saturation. In good seeing we obtained fewer photons per frame due to smaller stellar images. Also, when cirrus clouds were present we did not increase exposures times too much, to avoid over-exposed images from occasional holes in the clouds.

We have investigated in which conditions the photometry was worse than expected from photon noise alone. To do this we considered the ISIS1 photometry of stars from La Silla. We selected an ensemble of 19 bright stars and calculated their average scatter per night. The average flux for the ensemble was also derived and converted to a magnitude. One good night was chosen as the reference and the magnitude for that night was subtracted from the magnitudes for all other nights.

The measured rms scatter is plotted against the magnitude for all the nights in Fig. 6. If only photon noise were present the scatter should follow the solid line in Fig. 6, i.e., following the relation: $5\ \log_{10}\sigma = m - m_{\rm ref}$.

Most of the nights follow this law, but there are exceptions. Nights with a high sky background clearly stand out as having poorer photometric precision (diamonds in Fig. 6). A second problem arises when the seeing is very good because the images are under-sampled (triangles in Fig. 6).

An important issue is whether any of the three reduction techniques are superior. In general, we find similar results for the different techniques. However, MOMF is clearly not suited for crowded fields and only performs as well as ISIS and DAOPHOT for a small fraction of stars. The quality of the DAOPHOT photometry is comparable to the ISIS results, although ISIS is superior in the most crowded areas. We also find the best results with ISIS for faint stars, especially on nights with bad seeing. This is shown in Fig. 7, where we compare the rms scatter in data from one bad night from La Silla using DAOPHOT (left panel) and ISIS (right panel). The rms noise of the K giant stars is 40% lower for the ISIS reduction.

It is possible that with a more careful choice of PSF stars and other parameters involved in the DAOPHOT reductions, it may be possible to improve these results. The optimum choice of parameters for good observing conditions might not be the best for frames obtained under non-photometric conditions.

A final illustration of the differences between the algorithms is presented in Fig. 8. Here, the rms scatter is presented for three different reductions: ISIS1, ISIS2 and DAOPHOT. Each point is for a particular star and the symbols define which reduction technique was being used. It is evident that none of the techniques produce the best results in all cases, although the image subtraction method ISIS1 has been the most successful.

The time series from each observatory show different characteristics due to different observing conditions, telescopes and detector setups. At SSO the seeing was considerably worse, leading to more extended stellar images. This led to increased noise as a result of the higher influence of the background level, which is worse for fainter stars. This effect is shown in Fig. 9. The CTIO data are heavily influenced by the presence of the Moon close to the target field, particularly in the middle of the run, and this makes the data of rather poor quality. The results can be characterized by the rms noise per data point for a non-crowded K giants for the three sites on a good night: 1.6 mmag for La Silla, 3.0 mmag for CTIO and 2.1 mmag for SSO.

4. Light curve preparation

The outcome of the previous section is either absolute or differential magnitudes. In both cases, it is necessary to make differential photometry by comparing each target star with a set of reference stars. The effects of extinction, instrumental drifts and other sources of non-stellar noise need to be minimized for us to study any stellar signal at frequencies below 30 μHz, corresponding to periods longer than 9 h. The approach is described in the following sections.

4.1. Ensemble photometry

An ensemble of reference stars was used to derive the relative magnitudes for all stars, in order to remove transparency and extinction variations. In M 4 there is a wide range of possibilities for choosing reference stars. However, the results depend strongly on the method used to calculate the ensemble average.

The algorithm we employed was the following: for a given target star, a number of reference stars were selected, which were required to have similar V magnitude and $B - V$ colour to the target and be within a certain distance (e.g., half the size of the CCD). We calculated the magnitude difference between the target star and each reference star for a whole observing block ($t \geq 7$ d) and subtracted the median value, producing a time series $\Delta m_i(t)$, where the index i indicate the reference star.

We then did an analysis night by night. For each night, the rms noise $\sigma_{i,\rm rms}$ of each $\Delta m_i(t)$ time series was calculated and a weight assigned using

$$w_i = 1/\sigma^2_{i,\rm rms}. \quad (1)$$

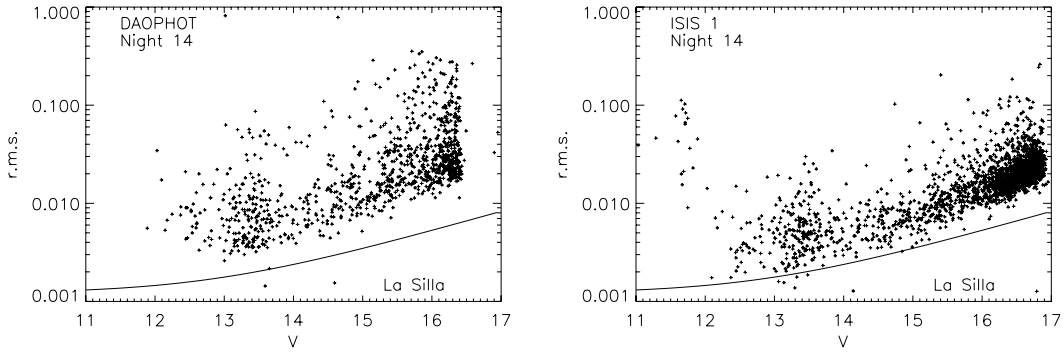

Fig. 7. The mean scatter per data point per night for night 14 for the DAOPHOT (*left panel*) and ISIS1 reduction (*right panel*). The line gives the noise level for a good night (see Fig. 4).

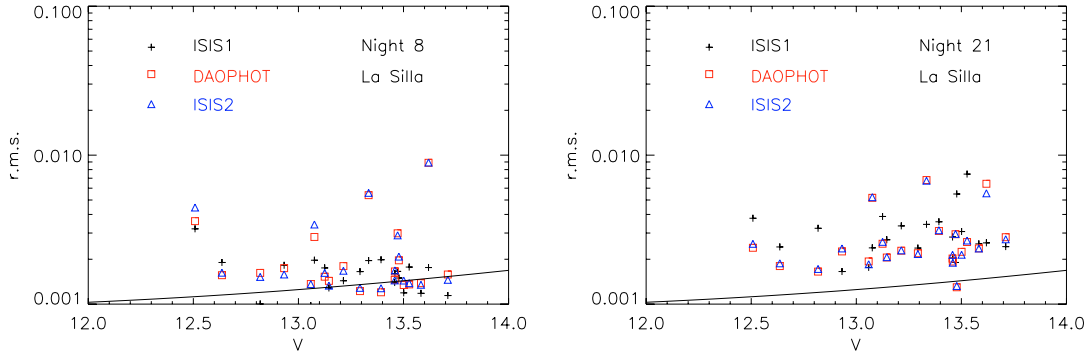

Fig. 8. The rms noise level in K giant stars for La Silla data from two different nights. The noise level from the three reduction methods is similar for most stars, but in a few cases the DAOPHOT and ISIS2 noise levels are higher than for ISIS1.

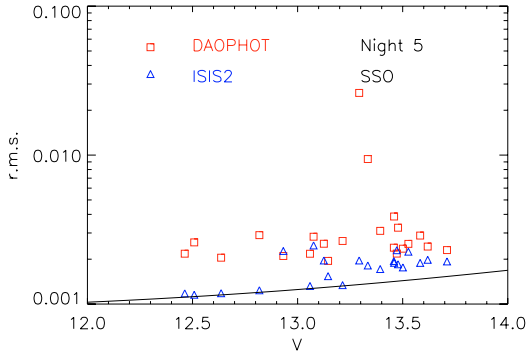

Fig. 9. The rms noise levels in data from a good night at SSO. DAOPHOT is doing significantly worse than ISIS2. Notice the increased noise at faint magnitudes relative to the photon noise estimate (solid curve).

The 10 stars with highest weights were used to calculate the final light curve for the night, as the weighted sum:

$$\Delta m(t) = \sum_{i=1}^{10} w_i \Delta m_i(t) / \sum_{i=1}^{10} w_i. \quad (2)$$

The set of reference stars varied from night to night. The method does not involve any high-pass filtering at a timescale of one day, since the median was subtracted before splitting the time series into single nights. The technique gives 10–20% lower white noise levels in the final light curves compared to the simpler choice of a common set of reference stars extending over all nights of an observing period. The final light curves were obtained by selecting, for each observing site, the result with lowest noise among the different methods applied (DAOPHOT, ISIS1 and ISIS2).

4.2. Decorrelation

Instrumental drifts and reduction noise may introduce correlations between the measured magnitudes and parameters such as the colour of the star, position on the CCD airmass and sky background. We found no clear correlations and so no decorrelation was performed.

4.3. Combining B, V and R

The result from the procedures described in Sect. 4.1 is a set of light curves from the three sites in three filters: B, V and R. In our search for solar-like oscillations in the K giants, we assumed that phase shifts between observations in different filters are small (Jiménez et al. 1999). We also assumed that the oscillation amplitudes scale inversely with wavelength as Eq. (8) and we therefore scaled the B and R time series relative to the V filter: scaling factors were 1.222 and 0.846. The weights, described in the next subsection, were also scaled with the inverse factor following Eq. (4).

4.4. Removing outliers and weighting the data

Due to the changes in observing conditions, there is a large variation in the data quality from night to night. It is therefore essential to apply weights when the Fourier spectra are calculated.

As a first step we removed obvious outliers. All points that deviated by more than 5σ from the mean were discarded. Weights were then calculated for each star by combining a weight for each night with a weight based on the point-to-point scatter. Each night received a weight of

$$w_1 = 1/\sigma^2_{\rm night}, \quad (3)$$

Table 2. The 24 K giants selected for detailed analysis. First block provides IDs and basic observational parameters. Second block gives stellar parameters. Third block presents the predicted asteroseismic parameters using Eqs. (5)−(8).

ID	ID2[a]	α_{2000}	δ_{2000}	V^b	$B-V^b$	$L/L_\odot$	$T_{\rm eff}{}^c$	$R/R_\odot$	$\delta L/L^d$	$\nu_{\rm max}^e$	$\Delta\nu_0^f$	$\omega_{\rm c}^g$
66	364	16 23 53.65	–26 33 55.0	12.93	1.263	143.0	4723	17.9	254	8.9	1.64	16.4
78	1715	16 23 32.46	–26 26 20.7	13.09	1.254	123.1	4741	16.5	227	10.5	1.86	19.4
83	689	16 23 27.34	–26 30 59.1	13.03	1.303	130.3	4637	17.7	247	9.2	1.67	16.9
84	264	16 23 54.72	–26 31 22.6	13.12	1.183	120.0	4903	15.2	209	12.2	2.10	22.3
126	NA	16 23 26.94	–26 30 43.9	13.28	1.267	104.1	4714	15.3	204	12.2	2.07	22.4
162	986	16 23 50.23	–26 29 28.0	13.41	1.181	92.4	4909	13.3	173	15.8	2.56	29.1
166	1753	16 23 22.96	–26 30 32.6	13.44	1.221	89.3	4815	13.6	176	15.3	2.48	28.2
181	NA	16 23 50.01	–26 32 21.5	13.46	1.209	88.0	4844	13.3	172	15.9	2.55	29.2
195	NA	16 23 47.55	–26 31 06.0	13.47	1.218	86.9	4822	13.4	172	15.8	2.54	29.1
200	NA	16 23 19.94	–26 32 40.1	13.54	1.203	82.0	4856	12.8	163	17.2	2.71	31.6
201	NA	16 23 53.03	–26 28 09.1	13.53	1.201	82.4	4861	12.8	163	17.2	2.71	31.6
210	NA	16 23 43.11	–26 28 08.8	13.52	1.190	83.4	4888	12.8	163	17.3	2.73	31.8
228	NA	16 23 47.84	–26 29 50.2	13.56	1.196	80.5	4873	12.6	160	17.7	2.78	32.6
229	NA	16 23 45.01	–26 33 58.3	13.57	1.227	79.4	4803	12.9	163	17.1	2.68	31.4
243	NA	16 23 21.77	–26 26 45.8	13.59	1.205	77.9	4851	12.5	158	18.0	2.81	33.1
244	NA	16 23 24.57	–26 31 10.6	13.64	1.226	74.6	4805	12.5	156	18.2	2.82	33.5
259	243	16 23 42.43	–26 33 18.6	13.75	1.177	67.6	4919	11.3	139	21.8	3.26	40.1
266	NA	16 23 48.97	–26 29 21.3	13.70	1.278	70.8	4691	12.8	158	17.7	2.73	32.4
268	331	16 23 41.72	–26 29 47.9	13.73	1.213	68.6	4834	11.8	145	20.2	3.06	37.2
270	540	16 23 47.83	–26 32 44.7	13.78	1.153	65.4	4976	10.9	133	23.5	3.45	43.1
280	463	16 23 32.34	–26 29 22.4	13.82	1.172	63.0	4931	10.9	131	23.6	3.46	43.4
285	305	16 23 42.13	–26 32 07.4	13.83	1.233	62.7	4788	11.5	139	21.4	3.18	39.3
292	1005	16 23 26.05	–26 30 39.6	14.03	1.172	51.9	4931	9.9	115	28.7	4.00	52.7
293	1059	16 23 22.50	–26 29 41.2	14.07	1.165	50.1	4947	9.7	111	30.0	4.15	55.2

[a] ID2 is from Stetson (2007) if present in the catalog (NA means not available).
[b] V and $B-V$ are calibrated using stars in the Stetson (2007) database.
[c] $T_{\rm eff}$ is found using the $B-V$ calibration of Alonso et al. (1999).
[d] Peak amplitude in ppm when assuming $\delta L/L \propto (L/M)^{0.7}$.
[e] $\nu_{\rm max}$ is the expected peak frequency for p-modes in μHz.
[f] $\Delta\nu_0$ is the large separation in μHz.
[g] $\omega_{\rm c}$ is the acoustic cutoff frequency in μHz.

where $\sigma_{\rm night}$ is the rms noise of the time series for the entire night.

The point-to-point weights were calculated by first fitting a spline to an averaged time series with a smoothing width of ±0.075 d and subtracting this from the data. The noise level, $\sigma_{\rm pt}$, at any each point time was then the average rms calculated using a Gaussian with a width of 0.05 d. The weight was chosen as the inverse of the noise level:

$$w_2 = 1/\sigma_{\rm pt}. \quad (4)$$

We note that the weighting in Eq. (4) (as opposed to the inverse variance) was also preferred for similar multi-site campaigns by Handler (2003) and Bruntt et al. (2007).

The final weight was the product of w_1 and w_2. A maximum weight (4 times the mean weight) was set to avoid nights with very few points being given very high weight.

5. Selection of K giant targets

We selected 24 K giants for a detailed analysis. The stars are found in the least crowded parts of M 4 and cover a range in luminosity on both sides of the bump stars. We selected stars with an rms scatter in the time series below 4 mmag. We list their ID numbers, standard V magnitude and $B-V$ colour in Table 2. The positions of some of the stars in the colour–magnitude diagram are shown in Fig. 2 and their positions in the cluster are marked with squares in Fig. 3.

To calculate $L/L_\odot$, $T_{\rm eff}$ and $R/R_\odot$ for the targets, we used cluster parameters from Ivans et al. (1999) for M 4: distance $d = 2.1$ kpc, reddening $E(B-V) = 0.37$, interstellar absorption $A_V = 4.0E(B-V)$, metal content [Fe/H] = −1.2, bolometric correction $BC = -0.48$ and mass $M = 0.85\ M_\odot$. As pointed out by Ivans et al. (1999), the reddening varies across the cluster. These parameters lead to a distance modulus of $(m-M)_V = 13.1$. This compares reasonably well with the mean magnitude of the RR Lyrae stars (Kopacki & Frandsen 2007) in the range 13.2−13.3, which have absolute magnitude $M_{\rm V} \simeq 0.0$. The uncertainty of the cluster parameters introduces a ∼10% uncertainty in the luminosities.

5.1. Expected signal for solar-like oscillations

We have estimated the amplitude and frequency that is expected for solar-like oscillations in each target. We used the following scaling relations for the frequency separation, $\Delta\nu_0$, the expected location of p-mode maximum frequency, $\nu_{\rm max}$, and the acoustic cutoff frequency, $\nu_{\rm ac}$:

$$\Delta\nu_0 = 134.9\ (M/M_\odot)^{1/2}(R/R_\odot)^{-3/2}\ \mu{\rm Hz}, \quad (5)$$

$$\nu_{\rm max} = 3050\ \frac{M/M_\odot}{(R/R_\odot)^2(T_{\rm eff}/5777\ {\rm K})^{0.5}}\ \mu{\rm Hz}, \quad (6)$$

$$\nu_{\rm ac} = 5600\ \frac{(M/M_\odot)}{(R/R_\odot)^2(T_{\rm eff}/5777\ {\rm K})}\ \mu{\rm Hz}. \quad (7)$$

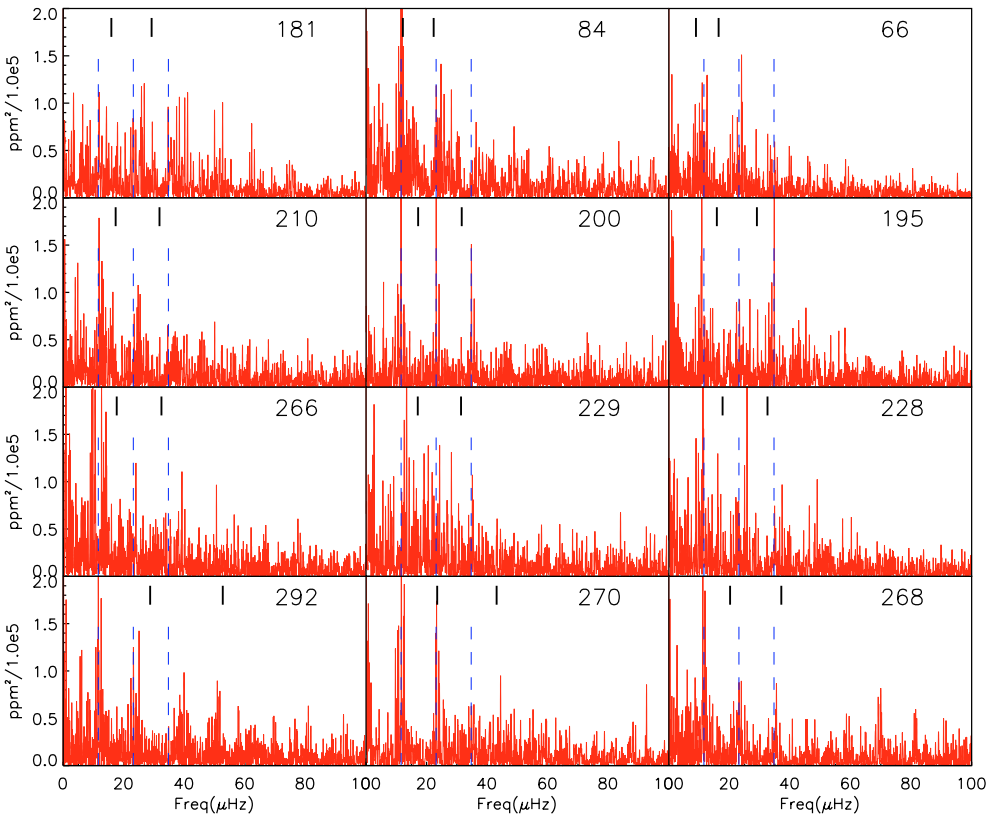

Fig. 10. Power spectra for the 12 K giants with the lowest noise at high frequencies. The luminosities of the stars increase from *left to right* and *bottom to top*. The predicted location of the maximum p-mode power and the acoustic cutoff frequency (indicated by thick black lines) shift to lower frequencies with increasing luminosity. Frequencies at multiples of 11.57 μHz (1 c/d) are indicated with vertical dashed lines.

The amplitudes of the oscillation modes were estimated from the calibration by Kjeldsen & Bedding (1995), but using the scaling $\delta L/L \propto (L/M)^{0.7}$ suggested by Samadi et al. (2007):

$$(\delta L/L)_\lambda = 4.7 \, \frac{[(L/L_\odot) \, / \, (M/M_\odot)]^{0.7}}{(\lambda/550 \text{ nm}) \, (T_{\rm eff}/5777 \text{ K})^2} \text{ ppm}. \quad (8)$$

The computed parameters using Eqs. (5)−(8) for the 24 selected K giants are listed in Table 2. As the luminosity decreases from about 150 to 50 $L_\odot$, the expected amplitudes decrease from 300 to 100 ppm, while the frequency of maximum power shifts from 9 to 30 μHz (periods of 31 to 9 h). The search for the signatures of the oscillations is difficult because we are in the region of the frequency spectrum that is affected by slow drifts originating from observing conditions (seeing, transparency and extinction) and the instrument (e.g., slight changes in the position of the stars on the CCD).

6. Time series analysis

6.1. Fourier analysis

The light curves were analysed using the Fourier analysis program PERIOD98 (Sperl 1998). In Fig. 10 we show the power spectra computed from the light curves using weights (see Sect. 4.4). The spectra of these 12 K giants cover a range in luminosity from 50 to 140 $L_\odot$, increasing from left to right and bottom to top.

In general the white noise increases as the stars become fainter but some stars have significantly higher noise than expected, which may indicate the presence of a close neighbouring star or an unidentified instrumental problem. The noise levels in the amplitude spectra lie in the range 60−100 ppm at 81−104 μHz (white noise), increasing to 100−140 ppm at 23−46 μHz. With this low noise level we would expect to detect oscillations if the amplitudes follow the extrapolations used in Sect. 5.1 (see Table 2), provided the mode lifetime is not as short as the few days found by Stello et al. (2006a). Stochastic excitation often gives rise to higher than average amplitudes for observing periods that do not exceed the lifetimes by large factors.

The highest peaks below the acoustic cutoff frequency $\nu_{\rm ac}$ range from 200 to 400 ppm in the spectra plotted in Fig. 10. We cannot claim that they are real, since the signal-to-noise is low ($S/N < 4$) in all cases. In a few stars we see suggestive evidence of power in the expected range (#181, #228 and #229) that does not coincide with multiples of 1 c/d, but due to the low S/N we cannot claim to have detected p-modes.

6.2. Quantifying the effect of the spectral window

The observing window will introduce frequency spacings that may be mistaken for those characteristic of solar-like oscillations. Note that the spectral window is slightly different for each star because the applied weights vary from star to star.

In Fig. 11 we show the autocorrelation function of the spectral window for star #181. This is representative and gives an idea of the effect of the complicated spectral window, which is due to gaps in the time series. The autocorrelation function has a very pronounced peak at 11.57 μHz due to the daily side lobes. In addition, a strong peak at ∼0.81 μHz is seen. The origin of the peak is found in the observing schedule, where dark time was not allocated to the project (Fig. 1). When searching for the presence of the large separation using the autocorrelation technique, this

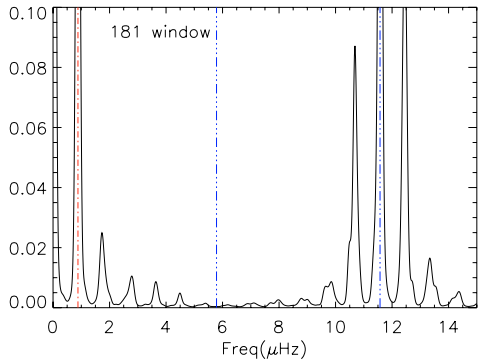

Fig. 11. The autocorrelation of the spectral window for star #181. The vertical lines indicate peaks at 11.57, 5.84 and 0.81 μHz (1, 0.5 and 0.07 c/d). Note that multiples of the 0.81 μHz peak are present.

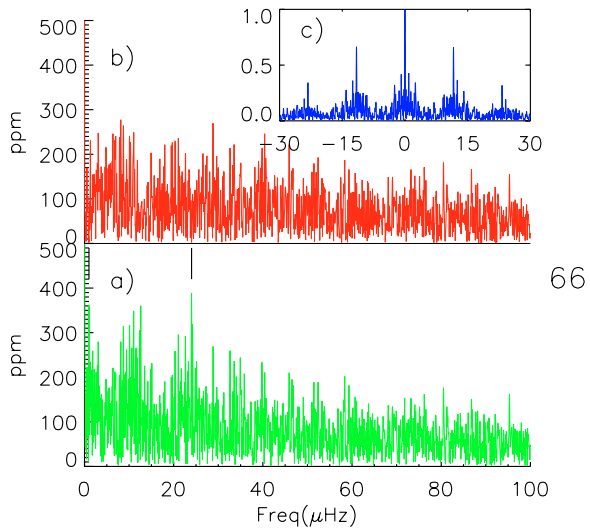

Fig. 12. Amplitude spectra for star #66, which is the brightest, non-saturated star in the subsample chosen for detailed analysis. Panel **a)** is the raw spectrum with one low frequency peak and a peak close to 2 c/d (23.14 μHz) marked. Panel **b)** shows the amplitude spectrum after subtracting the two peaks marked with vertical lines in panel **a)**. Panel **c)** shows the spectral window, which is seen to contain a complex substructure around each 1 c/d sidelobe.

will give rise to extra peaks. For a few stars the window function shows a more complex pattern giving rise to even more peaks in the autocorrelation. This will considerably reduce our ability to see clear evidence of stellar signal oscillations (see Sect. 7.1).

6.3. Subtracting 1 c/d aliases

We note that some of the observed excess peaks in the amplitude spectra are close to multiples of 1 c/d (11.57 μHz), as indicated by the vertical dashed lines in Fig. 10. These peaks are probably due to residual effects of extinction. In some light curves a peak in the range $\nu = 0.8-0.9$ μHz was also detected, which is probably caused by the spectral window (see Sect. 6.2). Therefore, following the approach of Stello et al. (2006b), we subtracted low-frequency peaks down to $S/N > 4$. We specify below whether we used the raw or the cleaned spectra (see Sect. 7).

In Fig. 12 we show an example of the process for star #66. Daily alias variations are seen in the amplitude spectrum in panel (a). Panel (b) is the amplitude spectrum after subtracting two peaks indicated by the vertical tick marks in panel (a). Panel (c) is the spectral window, which shows quite strong and complex sidelobes. The white noise level is ≃60 ppm and is calculated as the mean level in the frequency range 81−104 μHz.

6.4. Light curve simulations

To facilitate the interpretation of the observations in Sect. 7 we made simulations of the light curves. The time sampling and the noise properties are the same as for the observations and they include a known oscillation signal.

To mimic the noise we used the observed time series of two stars assuming that they resembled pure noise. The two stars (#66 and #292) are at either end of the luminosity range of the selected K giants. Both are among the K giant stars with the lowest noise in the amplitude spectra. The two stars show no clear evidence of power excess or a frequency separation that could arise from stellar oscillations.

We used different input amplitudes and mode lifetimes, using the simulation software described by De Ridder et al. (2006b) and Stello et al. (2004).

7. A search for evidence of solar-like oscillations

Inspection of the K giant amplitude spectra in Fig. 10 reveals that the noise increases towards low frequencies, indicating that drift noise is present in the light curves. This will seriously hamper the interpretation of the signal below ≃20 μHz. We see no clear evidence of excess power or the comb-like pattern expected for solar-like oscillations in any of the K giants. We do find clear evidence for an increase in excess power towards low frequencies, but it is not possible to disentangle drift noise from variations intrinsic to the K giant stars due to granulation or p-modes.

We have used two techniques to look for evidence of p-modes in the amplitude spectra:

- autocorrelation of the amplitude spectra to search for the large separation (Sect. 7.1);
- a search for evidence of excess power in the expected frequency range (Sect. 7.2).

7.1. Autocorrelation

Clear evidence for stellar oscillations would be a systematic behaviour in the observed frequency separations. The separation should increase with decreasing luminosity (Eq. (5)). In a few cases the autocorrelation shows a peak that could be indicative of the large separation. A prominent peak is seen in star #181, as shown in Fig. 13, where there is a peak at 2.75 μHz (predicted to be at 2.55 μHz). The highest peak at ≃0.9 μHz (vertical dashed line) is due to the window function (see Fig. 11) The autocorrelation was done on the raw spectrum. We find a few other stars with peaks in the autocorrelation spectrum that might come from the presence of a p-mode spectrum, but in the majority of cases we are not able to find a single prominent peak.

We made several simulations of stars #66 and #292 with various mode amplitudes and lifetimes, as described in Sect. 6.4. We used two methods to search for the known large separations of the inserted modes. The first was a simple autocorrelation while the second involved cutting the spectrum in small pieces and adding these together (forming a collapsed echelle diagram). The latter method is described by Christensen-Dalsgaard et al. (2007). Both methods gave similar results. For oscillations with

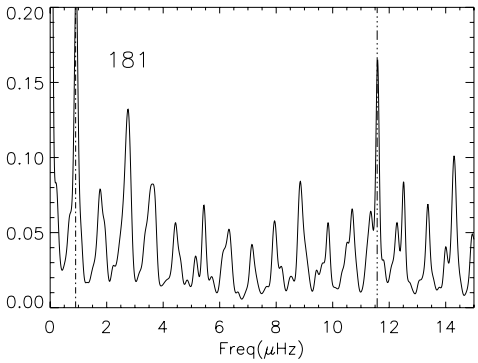

Fig. 13. The autocorrelation of the raw power spectrum for the giant star #181. Vertical lines represent peaks in the window function. The peak at 2.75 μHz could be the large separation, but might also be due to low frequency noise interacting with the window function.

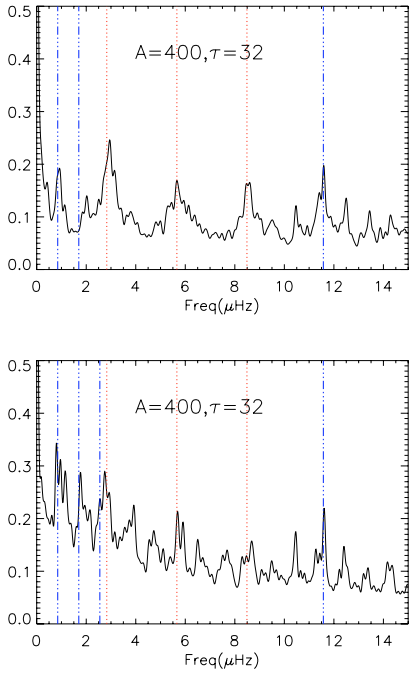

Fig. 14. Autocorrelation of a simulation of star #292 including oscillations. In the top panel the spectrum of #292 was cleaned for multiples of 1 c/d before adding the simulated signal and in the bottom panel, the same procedure was followed as for the observed time series data. The red dotted lines correspond to multiples of the large separation in the simulated signal. The blue vertical lines indicate parasitic peaks from the window function at 0.85 and 11.57 μHz (see Fig. 12).

a Q[1] value above 200, the correct large frequency separation $\Delta\nu_0$ was recovered in both stars for amplitudes down to 400 ppm.

In Fig. 14 we show the autocorrelation for star #292 after adding simulated oscillations with large separation 2.83 μHz, amplitude A = 400 ppm and lifetime τ = 32 d. We note that this lifetime is at least a factor two longer than expected. In the upper panel the spectrum of #292 was first cleaned for multiples of 1 c/d before adding the simulated signal. The autocorrelation clearly shows several peaks that correspond to multiples of the large separation present in the simulated signal (red dotted lines). The blue, dot-dash, vertical lines indicate aliases from peaks in the spectral window at 0.85 and 11.57 μHz (see Fig. 11). In the lower panel of Fig. 14, the procedure applied to the observed time series data was followed (see #181 in Fig. 13). In this case, the input large separation is much harder to recover.

[1] Q is the mode lifetime divided by the oscillation period, as used by Stello et al. (2006c) and presented for a set of stars in their Fig. 4.

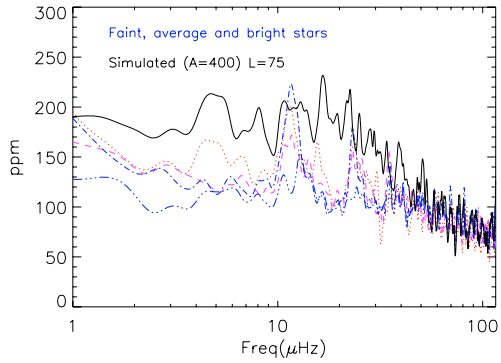

Fig. 15. Average smoothed spectra for three groups of observed K giants with luminosity $L \simeq$ 60, 80 and 130 $L_\odot$. The faint group (raw and clean version) are the blue lines, the average group is plotted as the magenta line and the bright group is the red line. The bottom curve is the faint group after multiples of 1 c/d are removed. The black solid line is for a simulation of star #292 with peak oscillation amplitudes of A = 400 ppm.

For the bright star (#66) the large separation is recovered for large Q values (>30) for inserted amplitudes as low as A = 200 ppm. However, if the lifetime is shorter than ≃16 days (Q < 12), we find that it is not possible to recover the input separation in any of the simulated series, even with amplitudes up to 800 ppm. Thus, our upper limits of 200−400 ppm only hold if the lifetime is greater than two weeks, as predicted by Houdek & Gough (2002) and Houdek (2006), and not a few days as found by Stello et al. (2006a).

7.2. A search for evidence of excess power

To search for excess power we followed the approach used by Stello et al. (2007) in their analysis of K giants in the open cluster M 67. The K giant stars in M 4 were divided into three groups with luminosities around 60, 80, and 130 $L_\odot$ (fainter, medium and brighter stars). For each group we calculated a mean raw amplitude spectrum. To demonstrate the effect of cleaning, we also produced a mean cleaned spectrum for the faint group.

In Fig. 15 we show the mean spectra. The raw spectra for the three groups of stars are quite similar, with prominent peaks near multiples of 1 c/d. This is unexpected and suggests that the power seen possibly is dominated by a noise component due to instrumental drift in the data.

Using the simulations described in Sect. 6.4, we probed our ability to identify an inserted oscillation signal. The black, solid spectrum in Fig. 15 is based on a mean of four time series of star #292 with the addition of simulated p-modes with lifetimes in the range 2−8 days and peak amplitudes of A = 400 ppm per mode. These values cover the range of expected lifetimes, and averaging four simulations removes some of the stochastic features of the oscillations. This artificial spectrum clearly lies above any of the observed mean spectra. Our conclusion is that excess power from p-modes with amplitudes A > 300 ppm would show up clearly in our observed spectra.

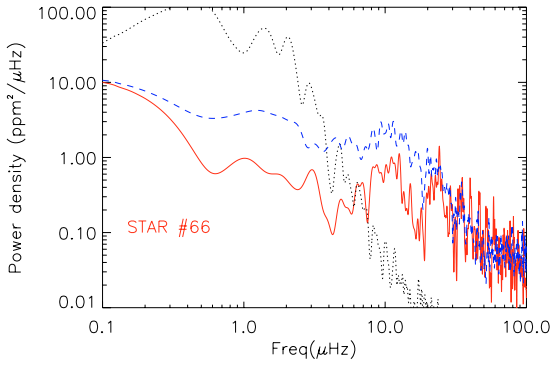

Fig. 16. Power density for three cases: 1) the observed star #66 (red, solid line), 2) a scaled power spectrum including granulation, p-modes with $A = 300$ ppm and white noise as star #66 (blue, dashed line), 3) the simulation by Svensson and Ludwig (2005) (black, dotted line).

8. Comparison with 3D-hydrodynamical simulations of granulation

We have compared our results for the K giants in M 4 with 3D hydrodynamical simulations of granulation by Svensson & Ludwig (2005). They modelled the effect of granulation using simulations of the convective motions in a box, which was scaled to predict observations of a spherical star. The results of Svensson & Ludwig (2005) indicate that K giants should have a low-frequency component of granulation power, similar to the levels achieved for some of the K giants in M 4.

One of their simulations (Ludwig 2006; kindly provided by G. Ludwig) is shown as the dotted black curve in Fig. 16. The stellar parameters are $R/R_\odot = 30.2$, $\log g = 2.0$, $T_{\rm eff} = 4560$ K, and metallicity [M/H] = 0.0. This corresponds to a luminosity $L = 385\ L_\odot$, which is larger by roughly a factor two than the brightest K giants we have observed. The larger luminosity means that the simulated granulation has larger amplitudes and excess power at lower frequencies than for our brightest target.

A scaling of the solar power spectrum has been attempted by Kjeldsen & Bedding (in preparation) and by Stello et al. (2007). A white noise component with the same level as the star chosen for comparison (#66) is added to a scaled granulation signal and a scaled p-mode spectrum. The scaling is very crude, and a difference of a factor two from our K giants would not be surprising. The granulation spectrum is shown in a logarithmic plot of power density in Fig. 16.

The simulated spectrum (black dotted line) and the scaled spectrum (blue dashed line) both show a larger power density at low frequencies than the observations (red solid line). The peak of the observed spectrum coincides with the peak around 10 μHz of the scaled spectrum, in which the power is due to the presence of oscillations. In the observed spectrum it is likely to be the 1 c/d alias.

Note that the 3D simulation (black dotted line) falls below the other curves at high frequencies because no white noise was included. The excess power at low frequencies in the 3D simulations is because the luminosity of the simulation model is twice that of star #66. The amplitude of the power density should scale with L^2 and the frequency with L^{-1}, which will bring the 3D simulations closer to the other curves, but still above the observations. Svensson and Ludwig (2005) showed that lowering the metallicity in a 1 $M_\odot$ model makes the power density drop considerably. The low metallicity of the cluster M 4 might explain the discrepancy between the observations and the 3D simulations.

9. Conclusion and discussion

We have presented results for a three-site multi-colour photometric campaign on the globular cluster M 4. We used data in the Johnson *BVR* bands from 48 nights with a time baseline of 78 days.

We compared the precision of the photometry obtained from three different photometric packages. In the most crowded parts of the field we found the best results using a difference image analysis (Alard 2000), while classical aperture photometry gave better results in the semi-crowded regions. The best photometry was found for stars not affected by crowding, in which case we achieved noise levels close to the theoretical limit.

The main goal of the campaign was to detect solar-like oscillations in the rich population of K giant stars in M 4. However, we are not able to claim an unambiguous detection and we summarize our conclusions here:

- We detect no individual peaks with $S/N > 4.0$.
- We find no significant large frequency separation from the autocorrelations of the amplitude spectra.
- We divided the stars with the best photometry in three groups and computed the average power spectra. From a comparison with realistic simulations of granulation and an assumed comb-like distribution of p-modes, we can exclude that power is present from p-modes with peak amplitudes above 300 ppm whatever the damping time. This upper limit is in accordance with the $(L/M)^{0.7}$ scaling suggested by Samadi et al. (2007), which predicts amplitudes below 300 ppm, for the most luminous stars, but far below the scaling law L/M from Kjeldsen & Bedding (1995).
- In all K giants, the amplitude spectrum rises towards low frequencies. This would be consistent with granulation, but we find that the observed increase does not vary with stellar luminosity. Thus we cannot differentiate between drift noise in the data and the expected granulation signal.
- We have compared the observations with a 3D-hydrodynamical simulation for solar metallicity. The observed power density at low frequencies is much lower than the simulations of granulations predict. In their 3D simulations, Svensson & Ludwig (2005) found that granulation power is substantially smaller for lower metallicity (M 4 has [Fe/H] = −1.2). This could explain why our measurements, even for the brightest star, fall considerably below the simulations (Fig. 16).

Our results support the recent evidence for short lifetimes in giant stars (Stello et al. 2006a) and contradict the theoretical predictions by Houdek & Gough (2002).

For the population II star ν Indi, which has a low luminosity (6 $L_\odot$), p-modes have been detected (Bedding et al. 2006; Carrier et al. 2007). While we cannot tell whether the stochastic driving still works in population II stars around $L = 100\ L_\odot$, we can say it cannot be very efficient and certainly does not exceed amplitudes expected from the $(L/M)^{0.7}$ scaling relation suggested by Samadi et al. (2007). This is contrary to the conclusion for the K giants in M 67 by Stello et al. (2007), who found indications of p-mode power in stars at lower luminosities (10−20 $L_\odot$). They found better agreement between observations and predictions if the amplitudes scale as L/M. Their noise level at low frequencies did not permit any statement for stars at luminosities similar to the stars investigated in M 4. It remains an open question whether the stochastic driving still works in population II K giants.

Based on the results obtained from large multi-site campaigns on M 67 and M 4, it seems difficult to get conclusive positive results about the stochastic oscillations and the granulation from ground-based photometry. Improvements can be made, but extinction and other atmospheric effects will always be a limiting factor, especially at the timescales of the K giants. It is also difficult to get a clean window function due to changing weather patterns for campaigns lasting several weeks, which are needed to study solar-like oscillations in K giant stars.

9.1. Directions for the future

If a new campaign is organized we recommend using a single filter, since colour information is not likely to be of a quality that can lead to mode identification. We found no use for the differences between the filters and we recommend that the *V* filter is used in the future; the *B* filter observations show strong colour-dependent extinction and the amplitudes will be very low in *R*.

From the ground, one would do better by organizing a long-term radial velocity campaign. One immediate advantage is that the noise from granulation is 10 times lower in velocity (Grundahl et al. 2007, their Fig. 1). One could observe several K giants during the night since the time scale of the oscillations is several hours. A dedicated network providing good time coverage would be needed in order to obtain a clean window function. The proposed SONG network (Grundahl et al. 2007) is an example of such a programme.

For rapidly rotating stars, where the broad spectral lines prevent precise velocity measurements, observations of solar-like oscillations can be made with photometry from space. Giants are among the targets for the new photometric satellite missions like CoRoT (Baglin et al. 2006) and the future Kepler mission (Christensen-Dalsgaard et al. 2007). The CoRoT mission observes each field for up to 150 days while the Kepler mission will cover many more targets in a single field for up to six years.

Acknowledgements. This work was supported by the Danish National Research Council and the Australian Research Council.

References

Alard, C. 2000, A&AS, 144, 363
Alard, C., & Lupton, R. H. 1998, ApJ, 503, 325
Alonso, A., Arribas, L., & Martinez-Roger, C. 1999, 140, 261
Baglin, A., Michel, E., Auvergne, M., et al. 2006, Proc. of SOHO 18/GONG 2006/HELAS I, Beyond the spherical Sun (ESA SP-624), ed. K. Fletcher, & M. Thompson, CDROM, 34.1
Barban, C., De Ridder, J., Mazumdar, A., et al. 2004, in Proceedings of the SOHO 14 / GONG 2004 Workshop (ESA SP-559), ed. D. Danesy, 113
Barban, C., Matthews, J. M., de Ridder, J., et al. 2007, A&A, 468, 1033
Bedding, T. R., & Kjeldsen, H. 2007, Comm. Asteroseismol., 150, 106
Bedding, T. R., Butler, R. P., Carrier, F., et al. 2006, ApJ, 647, 558
Bruntt, H. 2003, Ph.D. Thesis, University of Aarhus (Denmark)
Bruntt, H., Grundahl, F., Tingley, B., et al. 2003, A&A, 410, 323
Bruntt, H., Stello, D., Suárez, J. C., et al. 2007, MNRAS, 378, 1371
Buzasi, D., Bedding, T., & Retter, A. 2003, Solar and Solar-Like Oscillations: Insights and Challenges for the Sun and Stars, 25th meeting of the IAU, Joint Discussion 12, 18 July 2003, Sydney, Australia, 12
Carrier, F., Kjeldsen, H., Bedding, T. R., et al. 2007, A&A, 470, 1059
Christensen-Dalsgaard, J., Arentoft, T., Brown, T. M., et al. 2007, Comm. in Asteroseismology, 150, 350
De Ridder, J., Barban, C., Carrier, F., et al. 2006a, A&A, 448, 689
De Ridder, J., Arentoft, T., & Kjeldsen, H. 2006b, MNRAS, 365, 595
Döllinger, M. P., Pasquini, L., Hatzes, A. P., et al. 2005, The ESO Messenger, 122, 39
Edmonds, P. D., & Gilliland, R. L. 1996, ApJ, 464, L157
Frandsen, S., Carrier, F., Aerts, C., et al. 2002, A&A, 394, L5
Gilliland, R. L., Brown, T. M., Kjeldsen, H., et al. 1993, AJ, 106, 2441
Grundahl, F., Kjeldsen, H., Christensen-Dalsgaard, J., et al. 2007, Comm. Asteroseismol., 150, 300
Handler, G. 2003, Baltic Astron., 12, 253
Houdek, G. 2006, Proc. of SOHO 18/GONG 2006/HELAS I, Beyond the spherical Sun (ESA SP-624), ed. K. Fletcher, & M. Thompson, CDROM, 28.1
Houdek, G., & Gough, D. O. 2002, MNRAS, 336, L65
Ivans, I. I., Sneden, C., Kraft, R. P., et al. 1999, AJ, 118, 1273
Jiménez, A., Roca Cortés, T., Severino, G., & Marmolino, C. 1999, ApJ, 525, 1042
Kjeldsen, H., & Bedding, T. R. 1995, A&A, 293, 87
Kjeldsen, H., & Frandsen, S. 1992, PASP, 104, 413
Kopacki, G. 2000, A&A, 358, 547
Kopacki, G., & Frandsen, S. 2007, Comm. Asteroseismol., 150, 383
Ludwig, H. G. 2006, A&A, 445, 661
Samadi, R., Georgobiani, D., Trampedach, R., et al. 2007, A&A, 463, 297
Sperl, M. 1998, Comm. Asteroseismol., 111, 1
Stello, D., Kjeldsen, H., Bedding, T. R., et al. 2004, Sol. Phys., 220, 207
Stello, D., Kjeldsen, H., Bedding, T. R., & Buzasi, D. 2006a, A&A, 448, 709
Stello, D., Arentoft, T., Bedding, T. R., et al. 2006b, MNRAS, 373, 1141
Stello, D., Kjeldsen, H., Bedding, T. R., & Buzasi, D. 2006c, MmSAI, 77, 406
Stello, D., Bruntt, H., Kjeldsen, H., et al. 2007, 377, 584
Stetson, P. B. 1987, PASP, 99, 191
Stetson, P. B. 1990, PASP, 102, 932
Stetson, P. B. 1994, PASP, 106, 250
Stetson, P. B. 2007, `http://www.physics.mcmaster.ca/Globular.html`
Svensson, F., & Ludwig, H.-G. 2005, in Proc. 13th Cambridge Workshop on Cool Stars, Stellar Systems and the Sun (ESA SP-560), ed. F. Favata, G. Hussain, & B. Battrick, 979